Hindawi
Mathematical Problems in Engineering
Volume 2019, Article ID 1484098, 15 pages
https://doi.org/10.1155/2019/1484098

Research Article

Recrystallization Microstructure Prediction of a Hot-Rolled AZ31 Magnesium Alloy Sheet by Using the Cellular Automata Method

Ming Chen,[1,2] Xiaodong Hu,[2] Hongyang Zhao,[2] and Dongying Ju[2,3]

[1]*School of Mechanical Engineering and Automation, University of Science and Technology Liaoning, Anshan, Liaoning 114051, China*
[2]*Research Center of Roll Casting Technology for Magnesium Alloys, University of Science and Technology Liaoning, Anshan, Liaoning 114051, China*
[3]*Department of Materials Science and Engineering, Saitama Institute of Technology, Fusaiji 1690, Fukaya, Saitama 369-0293, Japan*

Correspondence should be addressed to Dongying Ju; judongying888@163.com

Received 29 March 2019; Revised 14 July 2019; Accepted 25 July 2019; Published 16 September 2019

Academic Editor: Mohamed Shaat

A large reduction rolling process was used to obtain complete dynamic recrystallization (DRX) microstructures with fine recrystallization grains. Based on the hyperbolic sinusoidal equation that included an Arrhenius term, a constitutive model of flow stress was established for the unidirectional solidification sheet of AZ31 magnesium alloy. Furthermore, discretized by the cellular automata (CA) method, a real-time nucleation equation coupled flow stress was developed for the numerical simulation of the microstructural evolution during DRX. The stress and strain results of finite element analysis were inducted to CA simulation to bridge the macroscopic rolling process analysis with the microscopic DRX activities. Considering that the nucleation of recrystallization may occur at the grain and *R*-grain boundary, the DRX processes under different deformation conditions were simulated. The evolution of microstructure, percentages of DRX, and sizes of recrystallization grains were discussed in detail. Results of DRX simulation were compared with those from electron backscatter diffraction analysis, and the simulated microstructure was in good agreement with the actual pattern obtained using experiment analysis. The simulation technique provides a flexible way for predicting the morphological variations of DRX microstructure accompanied with plastic deformation on a hot-rolled sheet.

1. Introduction

Compared with high-level faulted energy metals such as aluminium alloys, magnesium alloys are prone to dynamic recrystallization during hot deformation due to fewer slip systems, lower stacking fault energy, and faster grain boundary diffusion. As an important softening and grain refinement mechanism, dynamic recrystallization plays an important role in controlling the deformation structure, enhancing the plastic forming ability and improving the mechanical properties of magnesium alloys. However, as a widely used light metal, magnesium alloy has a complex nucleation mechanism. Considering the nucleation and growth characteristics of magnesium alloys, the recrystallization mechanism includes two categories [1, 2]: continuous dynamic recrystallization (CDRX) and discontinuous dynamic recrystallization (DDRX). CDRX forms near the grain boundary, where stress concentration is high and proceeds with small-angle grain boundary networks, which are called subgrains and that migrate and merge to form new large-angle grains. DDRX involves a bulging nucleation mechanism during the local migration of the original grain boundary, and the high-density dislocation region results in-grain boundary outbreak due to stress imbalance. Local migration results in bulging, and grain boundaries increase the orientation difference by absorbing lattice dislocations, eventually evolving into large-angle grain boundaries. In addition, another mechanism based on

rotational dynamic recrystallization exists, in which the additional internal stress between grains caused by deformation leads to local distortion of grain boundaries, and the subgrains are generated by dynamic recovery near the distorted grain boundaries. New dynamic recrystallization grains are formed around the grain boundaries through the migration of subgrain boundaries and the merging growth of subgrains. The nucleation and growth mechanism of dynamic recrystallization of magnesium alloys depend on the hot working conditions. Related studies [3, 4] have shown that the recrystallization of magnesium alloys at room temperature is due to DDRX and rotational dynamic recrystallization. The nucleation mechanism of magnesium alloys belongs to CDRX during the deformation at the temperature range of 200°C–250°C, and DDRX dominates in the hot compression at the temperature range of 300°C–450°C. Aiming at the traditional nucleation and growth mechanism of DDRX, Ding and Guo [5, 6] proposed the DRX nucleation model and successfully applied the CA method to a Ti-6Al-4V alloy. A new model [7] has been proposed to describe CDRX based on the dislocation density in the hot rolling of AZ31 magnesium alloys. Moreover, numerous DRX studies have been carried out for alloy microstructures [8, 9]. Manonukul and Dunne [10] investigated the initiation of DRX under the inhomogeneous stress state in pure copper. Goetz and Seetharaman [11] first used the CA method for DRX, and until now, their method is regarded as a flexible and effective approach that is widely used to simulate the DRX process of various metals [12–14]. Li et al. [15] simulated dynamic recrystallization in the deformation behavior of AZ80 magnesium alloys using the CA method via DEFORM-3D and suggested that the CA model is feasible for studying the DRX process of AZ80 alloys. Kugler and Turk [16] carried out a study on modeling dynamic recrystallization under multistage hot deformation and proposed that the post-dynamic softening strongly dependent on the strain rate. Yanagida and Yanagimoto [17] proposed a new method to estimate the kinetics of dynamic recrystallization using the flow curve of metal received by the hot compression test. However, only few papers discussed the magnesium alloy recrystallization via the CA method, especially the prediction of microstructure evolution.

As shown in Figure 1, magnesium alloys with HCP crystal structure can only start the basal slip system at room temperature. Although the prismatic slip and pyramidal slip system can be activated at high temperature, it is still difficult to process. If the stress direction of the crystal is at a certain angle to the basal plane, it will be beneficial to the processing. The unidirectional solidification method is preferred to obtain dendrite microstructures. In this method, the columnar dendrites are grown along the opposite direction of the heat flux to obtain a certain orientation of the columnar dendrite microstructures. Thereafter, the sheet is cut at certain angles to achieve heavy reduction rolling. Thus, the small recrystallization grains and the weakened texture for magnesium alloy sheets are available, as shown in Figure 1(c). Asynchronous rolling, channel angle pressing technology, and other processing methods were used for the same deformation principle by increasing single-pass reduction through shear deformation. The mechanical properties of magnesium alloys depend on the alloy grain size and texture, and the recrystallized grains significantly affect the plastic deformation process; that is, grain refinement affects the mechanical properties of magnesium alloys by improving their plastic deformation properties. This study aimed to obtain a complete dynamic recrystallization microstructure and prove that good performance of magnesium alloy sheets with fine grains can be obtained to improve the rolling deformability.

2. Constitutive Model

Sellars and Tegart [18] proposed the most widely used constitutive model to describe the relationship between flow stress, strain rate, and deformation temperature during thermal activation. McQueen and Ryan [19] first applied the constitutive equations coupled with an Arrhenius term to steel in hot rolling and forging. Bhattacharya et al. [20] developed a series of constitutive equations describing the dynamic recrystallization for AZ31 magnesium alloys. In general, the relationship between flow stress and strain rate can be described as follows:

$$\dot{\varepsilon} \exp\left(\frac{Q_a}{RT}\right) = A_1 \sigma^{n_1}, \tag{1}$$

$$\dot{\varepsilon} \exp\left(\frac{Q_a}{RT}\right) = A_2 \exp(\beta\sigma). \tag{2}$$

A high flow stress state can be expressed by using equation (1), and a low flow stress state can be expressed by using equation (2).

For the AZ31 magnesium alloy, McQueen et al. [21] reported that the relationship between strain rate and flow stress coupled with an Arrhenius term under the large deformation state can be expressed using the hyperbolic sine function, which can describe the relationship between flow stress, strain rate, and deformation temperature under arbitrary flow stress:

$$\dot{\varepsilon} \exp\left(\frac{Q_a}{RT}\right) = A[\sinh(\alpha\sigma)]^n, \tag{3}$$

where Q_a is the activation energy of deformation, $\dot{\varepsilon}$ is the strain rate, T is the absolute temperature, R is the gas constant, and σ is the flow stress. n_l and n are the stress indexes, α is a parameter of stress magnitude, and $\alpha = \beta/n_l$; A_1, A_2, A, and β are the material-related constants, which can be obtained by the following equation (4).

Neglecting the effect of the thermal deformation activation on the temperature during rolling process, the natural logarithm of equations (1)–(3) is taken, respectively, and the following results can be obtained:

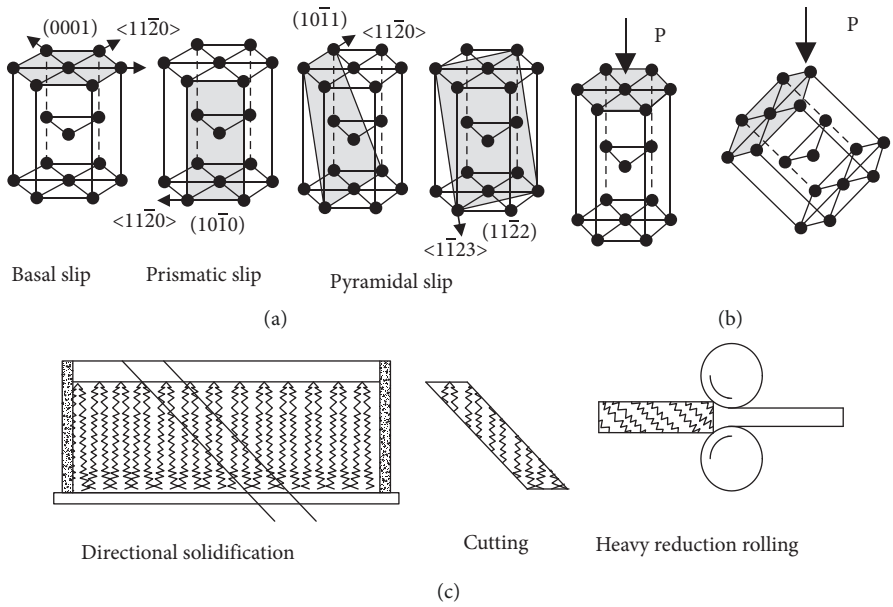

Figure 1: Processing sketch: (a) slip systems of magnesium; (b) load direction; (c) processing method of the unidirectional sheet.

$$\left.\begin{aligned} n_l &= \left|\frac{d\ \ln \dot{\varepsilon}}{d\ \ln \sigma}\right|_T \\ \beta &= \left|\frac{d\ \ln \dot{\varepsilon}}{d\sigma}\right|_T \\ n &= \left|\frac{d\ \ln \dot{\varepsilon}}{d\ \ln[\sinh(\alpha\sigma)]}\right|_T \\ \ln(A) &= \ln(\dot{\varepsilon}) - n\ln[\sinh(\alpha\sigma)] + \frac{Q_a}{RT} \\ Q_a &= R\left|\frac{\partial\ \ln \dot{\varepsilon}}{\partial\ \ln[\sinh(\alpha\sigma)]}\right|_T \left|\frac{\partial\ \ln[\sinh(\alpha\sigma)]}{\partial(1/T)}\right|_{\dot{\varepsilon}} \end{aligned}\right\}. \quad (4)$$

Figure 2 was obtained by fitting to the thermal compression test results, and by using linear regression, the following average values were obtained: $\beta = 0.054$, $n_l = 5.248$, $\alpha = 0.01\ \text{MPa}^{-1}$, $n = 6.25$, and $Q_a = 132.44\ \text{kJ/mol}$. From equation (4), the average intercept value of the relationship curve of Figure 2(c) can be calculated by $\ln(A) - (Q_a/RT)$, and the values of A at different temperatures can be obtained by it. The value of 1.8×10^{12} was set to A at the deformation temperature of 523 K in the recrystallization calculation programme.

The constitutive model of flow stress for a unidirectional sheet of the AZ31 magnesium alloy can be expressed as follows:

$$\dot{\varepsilon} = A[\sinh(0.01\sigma)]^{6.25} \exp\left(-\frac{132440}{RT}\right). \quad (5)$$

The Q value of 132.44 kJ/mol in this paper is near the lattice self-diffusion activation energy value of 135 kJ/mol, which can be used in the hyperbolic sine law to describe the flow stress of AZ31 alloys, proposed by Mirzadeh [22–24], and the Q value is slightly lower than that of the ordinary AZ31 magnesium alloy, which indicates that the hot deformation activation of directionally solidified sheet is easier.

3. CA Simulation

The kinetics of DRX associated with the thermomechanical processes was realized by changing the state variables of each cell based on specific rules. The matrix of continuous cells may be arranged in 1D, 2D, or 3D in the CA method. In most cases, the grids can be a triangle, square, or regular hexagon, and the 2D neighboring rules of von Neumann and Moore, which consider the nearest and second nearest neighbors, are often used. The cell space, neighborhood type, boundary conditions, and cell state are key elements for CA modeling. In the model, 2D square lattice and Neumann's neighboring rule were used, and we assumed that the dislocation density of the primary grains was uniform and identical in the rolling deformation microstructure. The initial dislocation density of the DRX microstructure was set as zero. Moreover, with the increasing rolling deformation, DRX occurs at the primary grain boundaries and the recrystallized grain boundaries when the dislocation density exceeds the critical value. A series of controlling equations was used to describe the nucleation of DRX and the growth of R-grains. The R-grains experience the nucleation state to the growth state, which were all controlled by the change of dislocation, and thus, the DRX process can be described by the following models.

In the course of numerical simulation of recrystallization, the following hypothesis was proposed: in this paper, the recrystallization nucleation is considered to be related to dislocation density and stress concentration and occurs at the grain boundaries. Therefore, a stress-related nucleation model was established, and the nucleation was judged by the accumulation of dislocation density. The

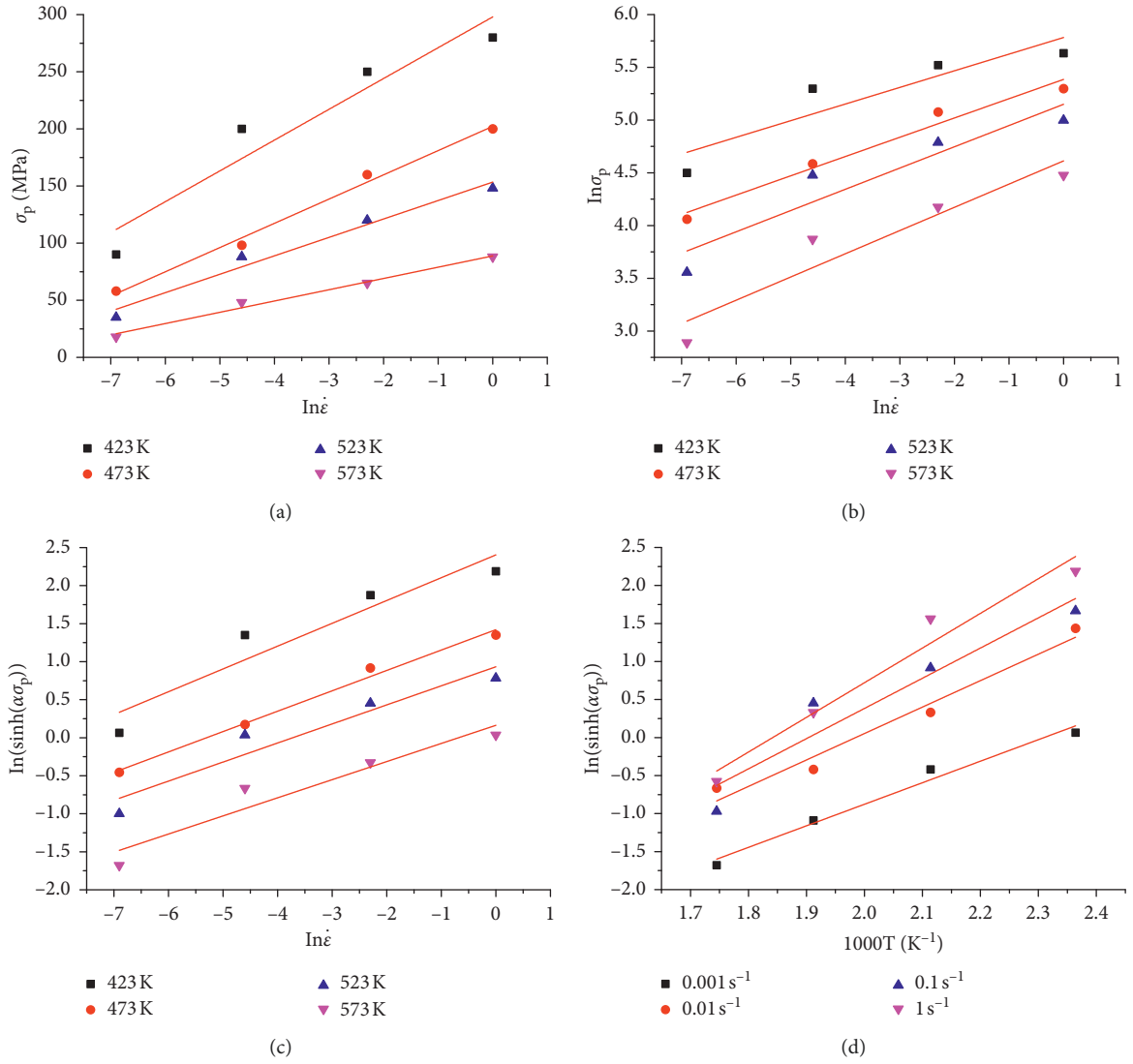

Figure 2: Relationship of deformation parameters for a unidirectional sheet of the AZ31 magnesium alloy: (a, b) relationship between the peak stress and the strain rate; (c) relationship between the strain rate and the peak stress of hyperbolic sine; (d) relationship between the peak stress and the deformation temperature.

primitive grain boundary is the main nucleation location of dynamic recrystallization. In CA simulation, only the grain boundary nucleation was considered, including primary grain boundary and new recrystallized grain nucleation. This hypothesis is based on the nucleation mechanism of the dynamic recrystallization boundary bulge.

3.1. Initial Microstructure. The initial microstructure of DRX was simulated using an improved CA method by considering the grain boundary mobility and the anisotropy of grain boundary energy [25, 26]. The simulated area covers $0.4 \times 0.4\,\text{mm}^2$, and the simulated area was divided into 400×400 grids. Thus, the corresponding size of each grid is $1 \times 1\,\mu m^2$. The periodic boundary condition and the Moore neighborhood rule were used in the simulated mesh model. At the beginning of the simulation, the cellular automata method was used to generate the initial structure. The 300 grains were set at the initial time, and each grain has a unique orientation ($1 \le S_i \le S_{\max}$, $S_{\max} = 180$). The cells with the same orientation in the initial structure will form one grain. The area of each grain was measured by the number of cells involved, and the equivalent diameter of the grain can be obtained by approximating the grain to a circle.

In each cellular automata time step, the two-dimensional matrix corresponding to the current microstructure was searched. When the cell S_i on the boundary was searched, a neighbor cell S_j was randomly selected from its neighborhood, and assuming that the state of the current cell S_i changes to the state of the cell S_j, the change of grain boundary energy ΔE was calculated:

$$\Delta E = E_{i,\text{new}} - E_{i,\text{old}},$$
$$E_i = \sum_{j=1}^{nn} J_i^j \left(1 - \delta_{s_i s_j}\right), \tag{6}$$

where

$$\delta_{S_iS_j} = \begin{cases} 0, & S_i \neq S_j, \\ 1, & S_i = S_j. \end{cases} \tag{7}$$

The grain boundary energy J_i^j between the cell i and the cell j is in accordance with the Read–Shockley equation [27] as follows:

$$J_i^j = \begin{cases} J_m \dfrac{\theta^\wedge}{\theta^*}\left[1 - \ln\left(\dfrac{\theta^\wedge}{\theta^*}\right)\right], & \theta \le \theta^*, \\ J_m, & \theta > \theta^*, \end{cases}$$

$$\theta^\wedge = \begin{cases} \theta_{ij}, & 0 \le \theta \le \pi, \\ 2\pi - \theta_{ij}, & \pi < \theta \le 2\pi, \end{cases} \tag{8}$$

$$\theta_{ij} = 2\pi \cdot \frac{\left|S_i - S_j\right|}{S_{\max}},$$

$$J_m = \frac{\mu b \theta^*}{4\pi/(1-\nu)},$$

where J_m is the large-angle grain boundary energy of AZ31; $\theta^\wedge$ is the orientation difference angle of adjacent grains; J_m and θ^* are the boundary energy and critical misorientation, respectively, when the grain boundary becomes the large-angle boundary; θ^* was set to 15°; μ is the shear modulus; b is the Burgers vector of dislocations; and ν is the Poisson ratio.

Based on the anisotropy principle, the grain boundary mobility [28] between the adjacent grains was calculated as follows:

$$M = \begin{cases} M_{\mathrm{m}}\left[1 - \exp\left(-5 \cdot \left(\dfrac{\theta^\wedge}{\theta^*}\right)^4\right)\right], & \theta \le \theta^*, \\ M_{\mathrm{m}}, & \theta > \theta^*, \end{cases} \tag{9}$$

where M_{m} is the maximum mobility corresponding to random large-angle boundary and M_{m} was set to 1 in the procedure.

The probability of transition from cell S_i to cell S_j was calculated as follows:

$$P = \begin{cases} 0, & \Delta E > 0, \\ \dfrac{M\left(S_i, S_j\right)}{M_{\mathrm{m}}}, & \Delta E \le 0. \end{cases} \tag{10}$$

After the transition probability was determined, a random number Rand $(0 \le \mathrm{rand} \le 1)$ was generated. If $P >$ rand, the transition is successful; otherwise, the state remains in the original orientation.

3.2. Dislocation Model. During the hot rolling process of the AZ31 magnesium alloy, the change of dislocation density was mainly determined using two competing processes of work hardening and recovery softening. According to the KM phenomenological model proposed by Mecking and Kocks [29], the expression of dislocation density varying with strain can be expressed using the derived method of equation (11) as follows:

$$\frac{d\rho}{d\varepsilon} = k_1\sqrt{\rho} - k_2\rho, \tag{11}$$

where ε is the strain, $k_1 = 2\theta_0/\alpha\mu b$ is the constant that denotes work hardening, $k_2 = 2\theta_0/\sigma_{\mathrm{s}}$ is the softening parameter that denotes recovery of dislocations, and α is a dislocation interaction term, which is around 0.5 for the magnesium alloy. In addition, θ_0 is the hardening rate, which is attached to the slope of the experimental flow stress-strain curve in the second stage of work hardening; and σ_{s} is the steady stress.

3.3. Nucleation Model. The nucleation process of dynamic recrystallization is accompanied by the accumulation of dislocation density. Nucleation begins only when the dislocation density reaches the critical value ρ_{c} and usually occurs at the grain boundary and in-grain defects. This paper only considered the nucleation at the grain boundaries and neglected the effect of crystal defects on nucleation. According to the widely used nucleation model $\dot{n} = C\dot{\varepsilon}\exp(-Q_{\mathrm{a}}/RT)$ proposed by Ding and Guo [5] coupled with the flow stress equation (5), the nucleation equation for the unidirectional sheet of the AZ31 magnesium alloy was set up and can be expressed using the following equation:

$$\dot{n} = C\left\{A[\sinh(0.01\sigma)]^{6.25}\exp\left(-\frac{132440}{RT}\right)\right\} \cdot \exp\left(-\frac{Q_{\mathrm{a}}}{RT}\right), \tag{12}$$

where C is a constant and Q_{a} is the activated nucleation energy. Considering the energy change, Roberts and Ahlblom [30] found that the critical dislocation density on the grain boundary can be calculated using the following equation:

$$\rho_{\mathrm{c}} = \left(\frac{20J_m\dot{\varepsilon}}{3blM_0{}^2\tau^2}\right)^{1/3}, \tag{13}$$

where $\tau = c\mu b^2$ and l are the line energy and mean free path of the grain dislocation, respectively; c is a constant, which was set to 0.5 in this study. M_0 is the DRX grain boundary mobility.

3.4. R-Grain Growth Model. The growth of the grain ensued after recrystallization nucleation. The essence of grain growth is the migration of large-angle grain boundaries. The driving force of grain growth depends on the dislocation density difference between the parent grain and the recrystallized grain. For the i recrystallized grains, the growth rate V_i is as follows:

$$\left.\begin{aligned} V_i &= \frac{M_0 F_i}{4\pi r_i^2} \\ F_i &= 4\pi r_i^2 \cdot \tau \cdot \Delta\rho_i - 8\pi r_i J_i^j \\ M_0 &= \frac{b\delta D_{0b}}{kT} \exp\left(-\frac{Q_b}{RT}\right) \end{aligned}\right\}, \quad (14)$$

where F_i is the driving force for the ith R-grain with the radius of r_i and $\Delta\rho_i$ is the dislocation density difference between the two neighboring cells. T is the absolute temperature, R is the gas constant, δ is the characteristic grain boundary thickness, D_{0b} is the boundary self-diffusion coefficient, Q_b is the boundary diffusion activation energy, and k is Boltzmann's constant. The required physical parameters [31] in the simulation are shown in Table 1.

Also, in the calculation for grain dimensions, we considered the 2D simulations as the cross section of a 3D microstructure, and the sphere radius R_r of equivalent average recrystallized grain can be calculated as follows [32]:

$$R_r = \frac{\sum_{i=1}^{N_r} \sqrt{S_i/\pi}}{N_r}, \quad (15)$$

where S_i is the recrystallized grain area and N_r is the recrystallized grain number.

The flow chart of the CA simulation for DRX is shown in Figure 3, and the simulated microstructure is shown in Figure 4.

4. Simulation Results and Discussion

In this paper, the DRX microstructural evolution of the AZ31 magnesium alloy was simulated under the large reduction rolling deformation using the CA algorithm. The total area was meshed using a 400×400 square lattice in the simulation, and the simulation region corresponds to a real square lattice of $1\,\mu m \times 1\,\mu m$, denoting the real dimension of the DRX microstructure. An angle within the range of 0°–180° was randomly set to the orientation of every primary grain.

Figure 5 shows a schematic diagram of macro-micro coupling analysis. Figures 5(a) and 5(b) show the stress and strain results, respectively. The stress and strain results are taken as boundary conditions and imported into the numerical simulation of micro-recrystallization, which directly affect the dislocation density and the recrystallization structure. The stress and strain distributions were calculated by using the finite element method, and the finite element analysis was coupled with the CA simulation. The stress results were inducted into equation (12), which determined the nucleation process. The strain results were set as the input of process parameters that directly affect the accumulation of dislocation density. In the DRX microstructural evolution process, the white regions represent the deformed matrix, the colored regions refer to the R-grains, and the black lines denote the grain boundaries. The grains, including the deformed matrix and R-grains, were vertically compressed, and the grain boundaries evidently became elongated, which is normal to the compression direction with the continuous rolling deformation. Considering that the nucleation of DRX may occur at the grain and R-grain boundary, the elongated grain boundary should affect the mean grain size and the kinetics of DRX.

In the finite element analysis, the actual sizes (the thickness is 3 mm) were used in the simulation. The reduction was set to 50%; the rolling speed was 0.45 m/s; the roller diameter was 130 mm; and the deformation temperature was 553 K. The effect of the width direction was ignored because the magnesium sheet is very thin, which can be attributed to the plane strain problem. Thus, the 2D simulation was adopted. The explicit dynamic algorithm was used in the simulation process. The required physical parameters in the finite element simulation are shown in Table 2.

The results of stress and strain obtained by finite element analysis are taken as the initial boundary conditions for recrystallization calculation and input in the "INPUT OF PROCESS PARAMETERS" of program diagram as shown in Figure 3. Considering the calculating ability of micro-recrystallization, only the recrystallization structure under two typical strain conditions are analyzed in the recrystallization analysis as shown in Figure 6.

The CA program was used to simulate the nucleation and grain growth to analyze the microstructure evolution affected by the strain rate. At 280°C rolling temperature, the grain growth increased as the strain rate decreased, as shown in Figure 6. Figure 6(a) shows the recrystallization microstructure at a strain rate of $0.1\,s^{-1}$, and the growing and migrating grains completely occupied the square area. Also, the percentage of DRX was almost 100%. In the CA simulation, the strain of the deformation zone was just 0.337, which is consistent with the strain results of the stable rolling zone determined using the finite element analysis shown in Figure 5. Furthermore, at a strain rate of $0.3\,s^{-1}$, the nucleation decreased because no sufficient time was available for the growth of DRX in the period of grain growth. The percentage of DRX was almost 70%, as shown in Figure 6(d). Clearly, the strain rate is an important factor that affects the nucleation and growth of R-grains. Therefore, the roller velocity can be set to obtain the different values of the stress and the strain rate, and thus, the optimized rolling process parameters can be achieved.

As shown in Figures 5 and 7, when the stress increased from 0 MPa to 170.8 MPa, the percentage of DRX significantly increased, and the mean grain decreased from 14.38 μm to 6.71 μm. The size distribution of initial grains and DRXed grains is shown in Figure 7, and clearly, stress is an important factor that affects the nucleation and growth of R-grains.

Figure 8 shows the influence of the rolling deformation temperature on the DRXed microstructure. The temperature notably has double effects on the grain size. On the one hand, the temperature provides the essential deformable energy for the nucleation and the growth of DRX. On the other hand, a high temperature results to a large grain size. At 200°C

Table 1: Physical parameters of the AZ31 magnesium alloy used in the CA simulation.

Properties	Value	Unit
T_m	473–673	K
b	3.21×10^{-10}	m
μ	1.7×10^{10}	$N \cdot m^{-2}$
D_0	1.0×10^{-4}	$m \cdot s^{-1}$
δD_{0b}	5.0×10^{-12}	$m^3 \cdot s^{-1}$
Q_a	132.44	$kJ \cdot mol^{-1}$
Q_b	92	$kJ \cdot mol^{-1}$

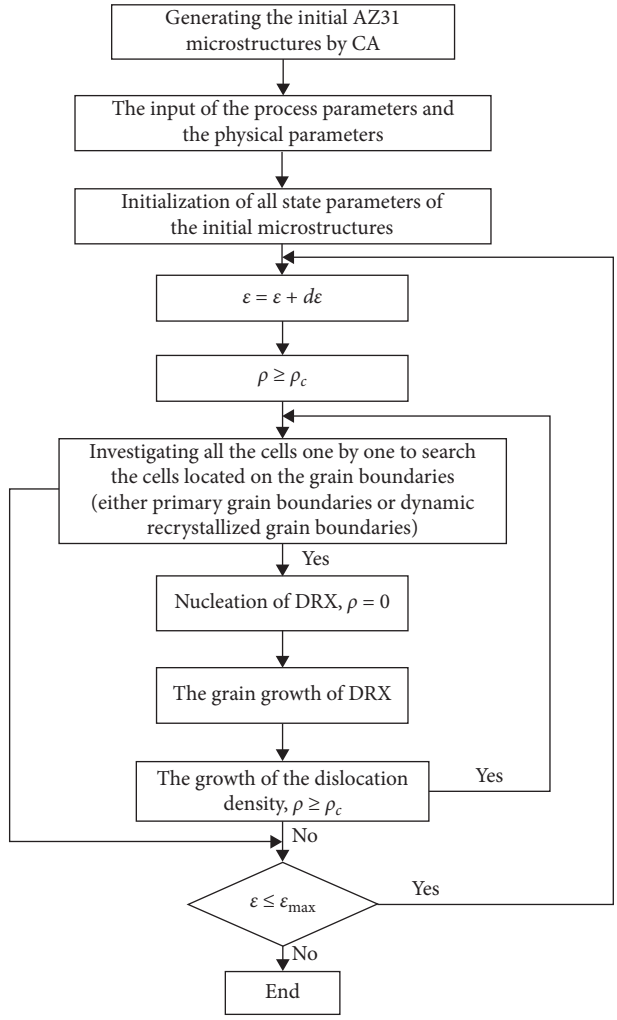

Figure 3: Flow chart of the CA simulation for DRX.

rolling temperature, the nucleation of DRX started at the grain boundary, which has a minor effect on the grain size, as shown in Figure 8(a). When the temperature increased, the DRX began to grow and refine the grain, as shown in Figure 8(b). At 280°C deformation temperature, the complete DRX microstructure was achieved, and DRX grains were refined, as shown in Figure 8(b). However, if the temperature is further increased, large coarse grains will be generated by the grain boundary driving force, as shown in Figures 8(c) and 9. Results show that with the increase of temperature, the recrystallization strengthened. The recrystallization of the large grain devoured the small grain around, and the overall size became larger, which is not conducive to grain refinement. Thus, strictly controlling the recrystallization temperature is needed to obtain the fine recrystallized organization.

Figure 9 depicts the process of grain reenlargement at high temperatures. In the early stage of recrystallization, the initial large grains become small recrystallization grains as shown in Figures 9(a) and 9(b). But, at the later stage, the

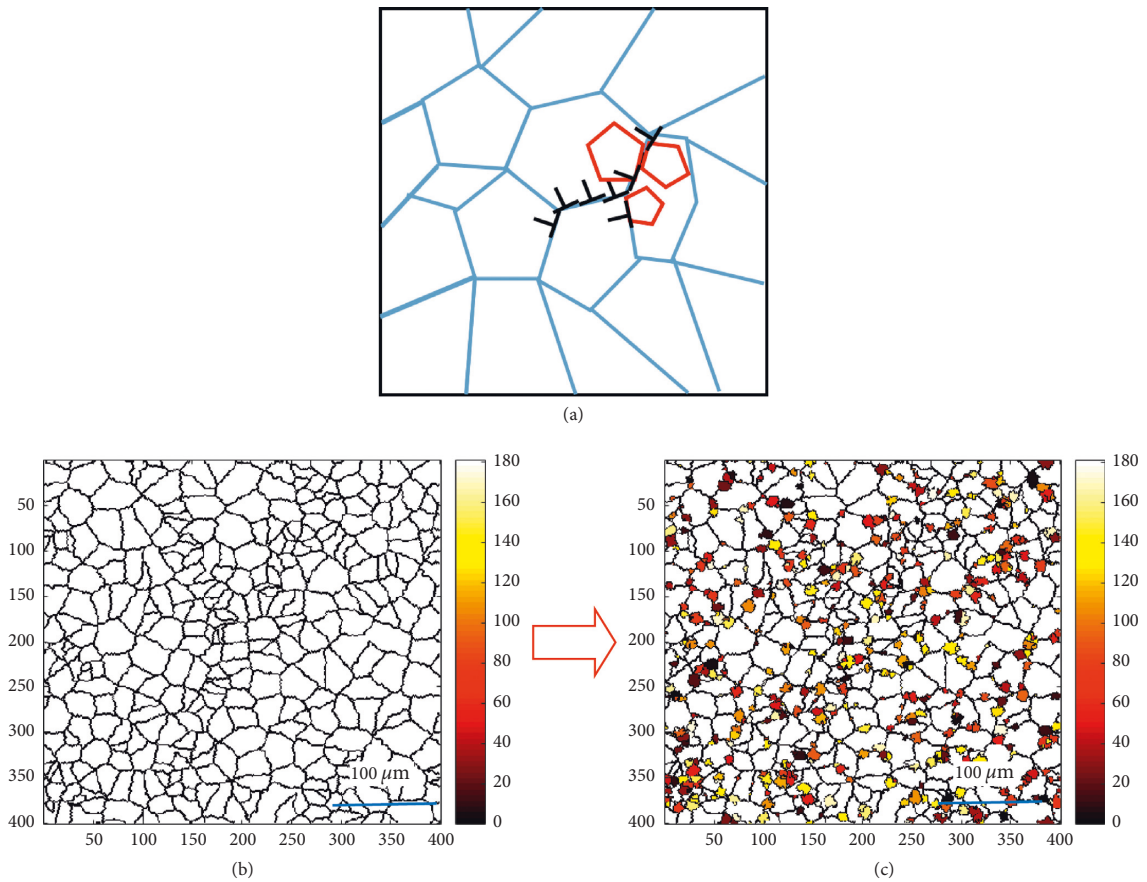

Figure 4: DRXed microstructure by CA method: (a) DRX nucleation principle; (b) simulation of initial microstructure by the CA method; (c) simulation of DRX microstructure by the CA method.

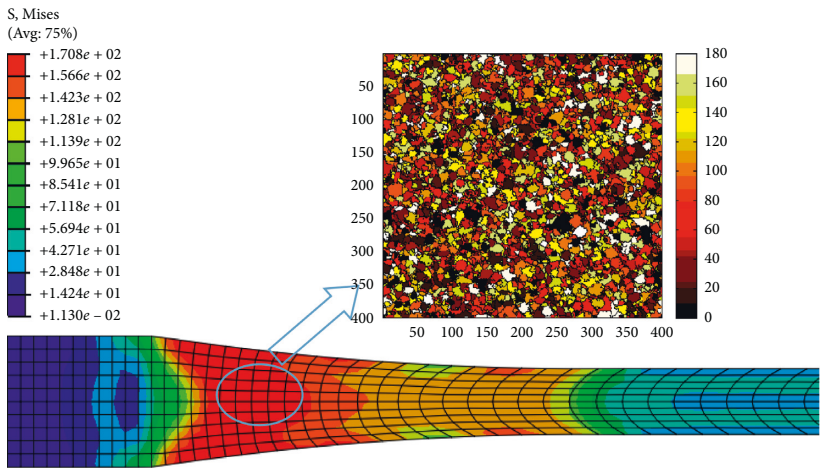

(a)

Figure 5: Continued.

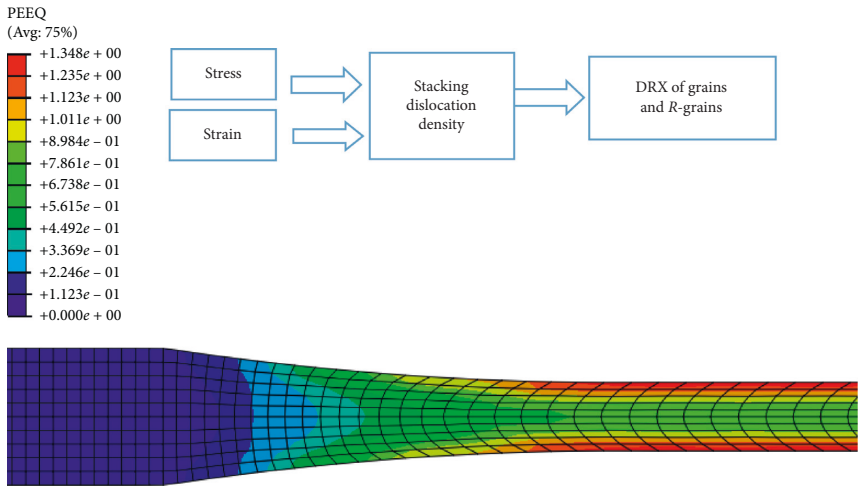

(b)

Figure 5: The schematic diagram of macro-micro coupling analysis.

Table 2: Physical parameters of the AZ31 magnesium alloy used in the finite element simulation.

Parameters	Value	Unit
Density	1.74×10^3	$Kg \cdot m^{-3}$
Alloy sheet temperature	553	K
Roller temperature	473	K
Thermal conductivity between roller and sheet	11	$kW \cdot (m^2 \cdot K)^{-1}$
Thermal convection coefficient between roller and air	0.016	$kW \cdot (m^2 \cdot K)^{-1}$
Stefan–Boltzmann constant	5.67×10^{-11}	$kW \cdot (m^2 \cdot K^4)^{-1}$
Emissivity	0.25	—
Dynamic friction coefficient	0.3	—

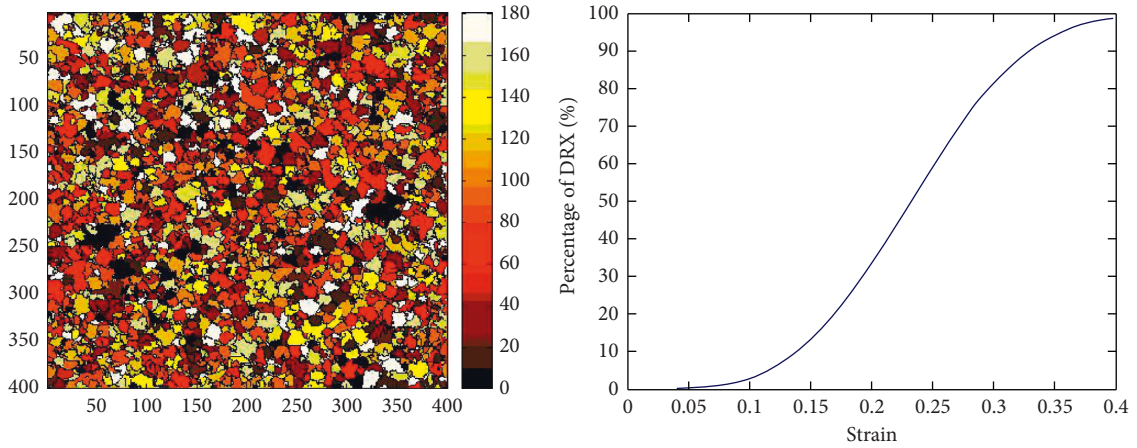

(a) (b)

Figure 6: Continued.

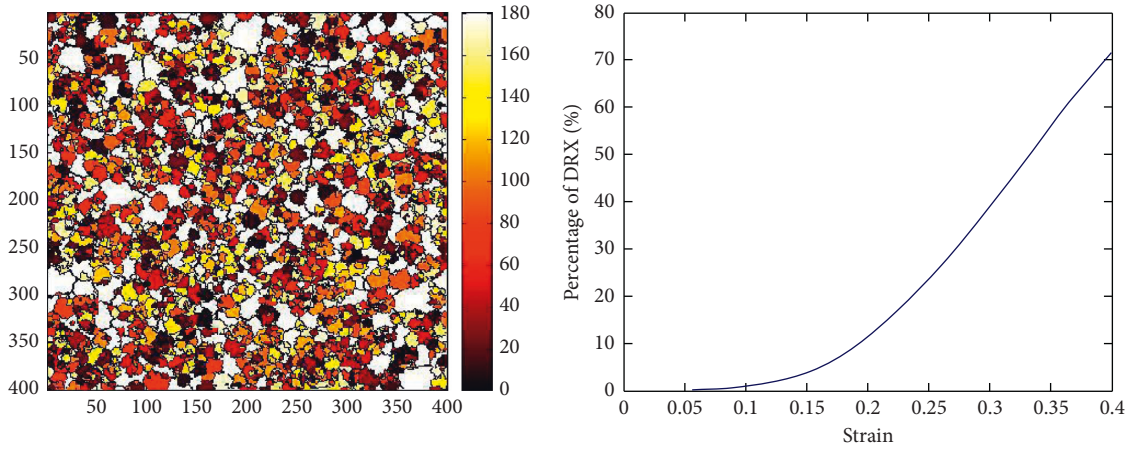

Figure 6: Simulated microstructure evolution of AZ31 magnesium alloy DRX at a strain of 0.34 and temperature of 280°C. Strains: (a, b) $\dot{\varepsilon} = 0.1$; (c, d) $\dot{\varepsilon} = 0.3$.

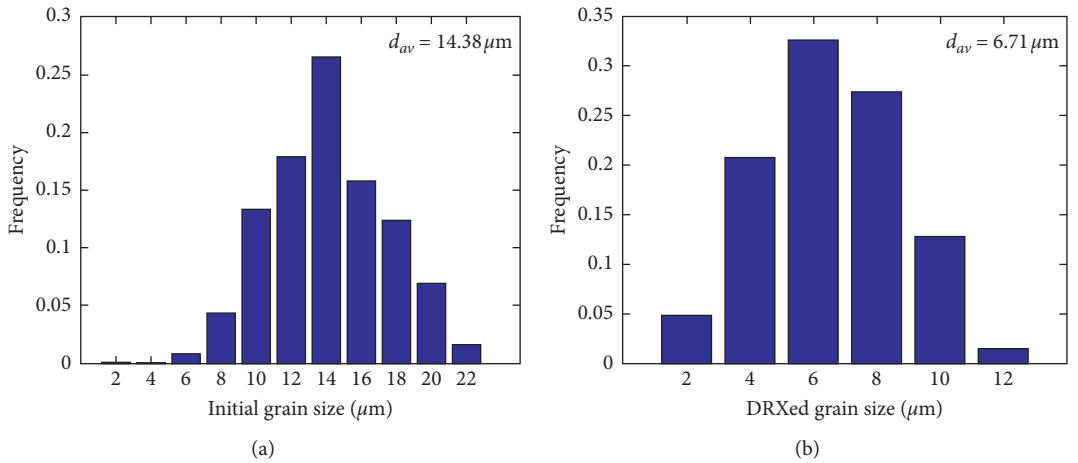

Figure 7: Initial grain size and DRX grain size (280°C of the rolling temperature).

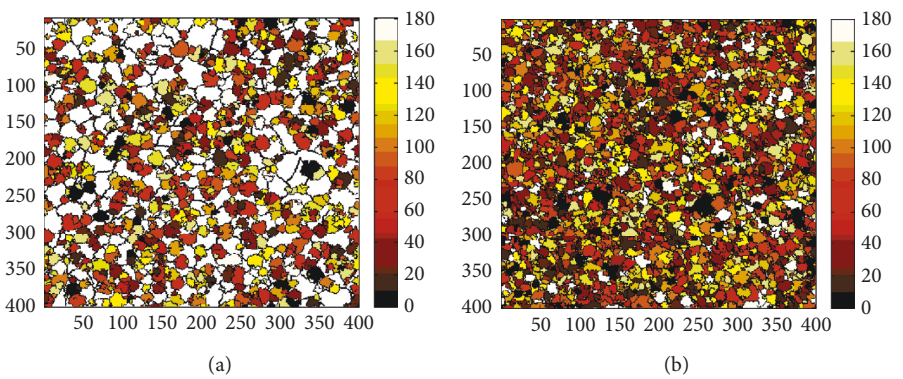

Figure 8: Continued.

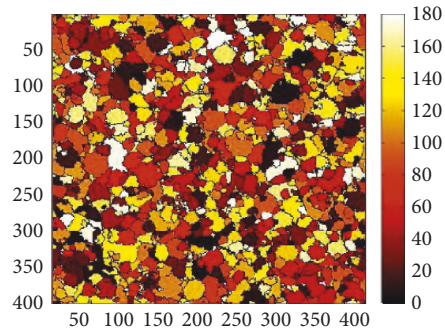

Figure 8: Simulated microstructure evolution of AZ31 magnesium alloy RX at a strain of 0.37 and a strain rate of $0.3\,s^{-1}$ in different temperatures: (a) $T = 200^{\circ}C$, (b) $T = 280^{\circ}C$, and (c) $T = 400^{\circ}C$.

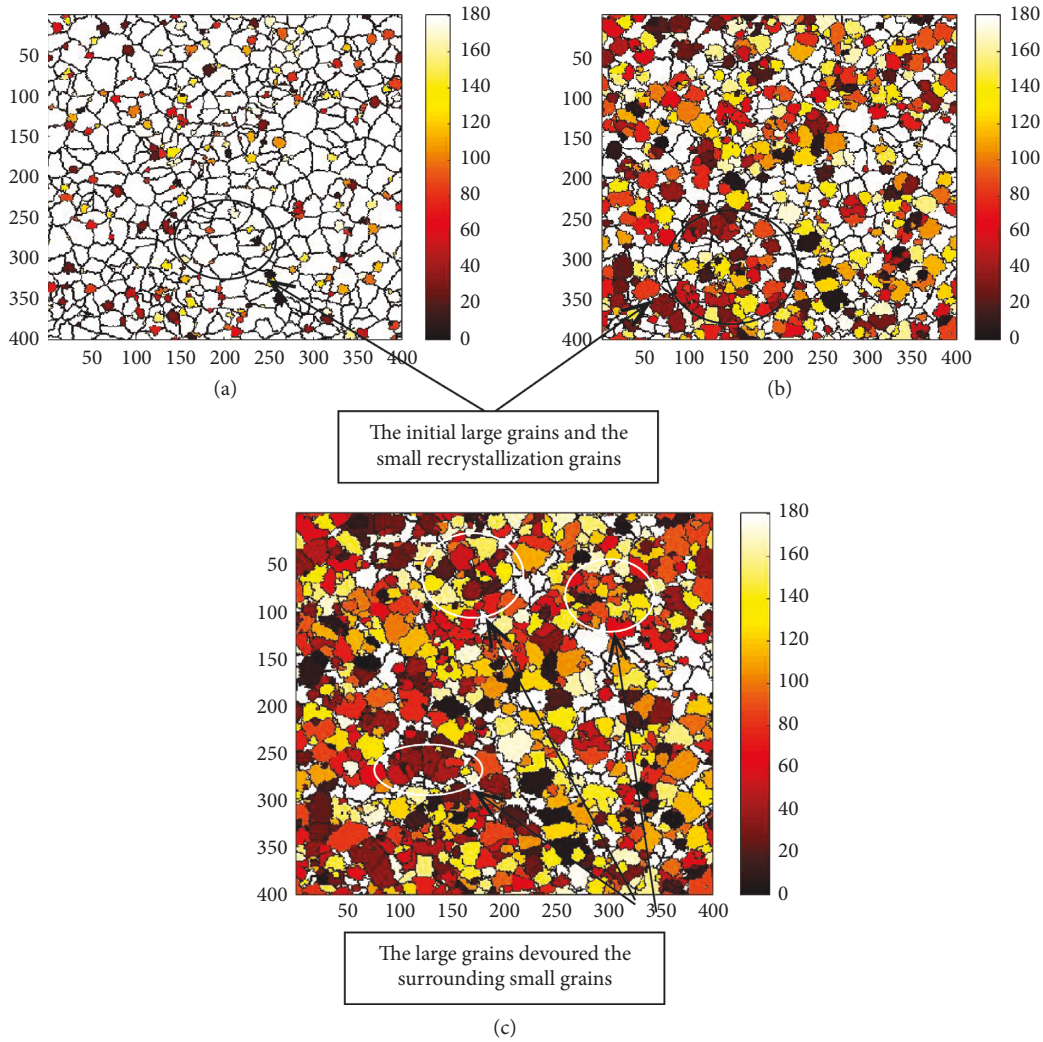

Figure 9: Simulated microstructure evolution of AZ31 magnesium alloy DRX at a strain of 0.4 and temperature of $400^{\circ}C$.

large grains devoured the small grains around and, then, made the grain size bigger again as shown in Figure 9(c). Therefore, the temperature is one of the important factors affecting recrystallization grain size.

The mean sizes of the R-grains, which are necessary to describe DRX, decreased with increasing temperature when a sufficient DRX microstructure is formed. Figures 7–9 evidently show that the mean sizes of the R-grains

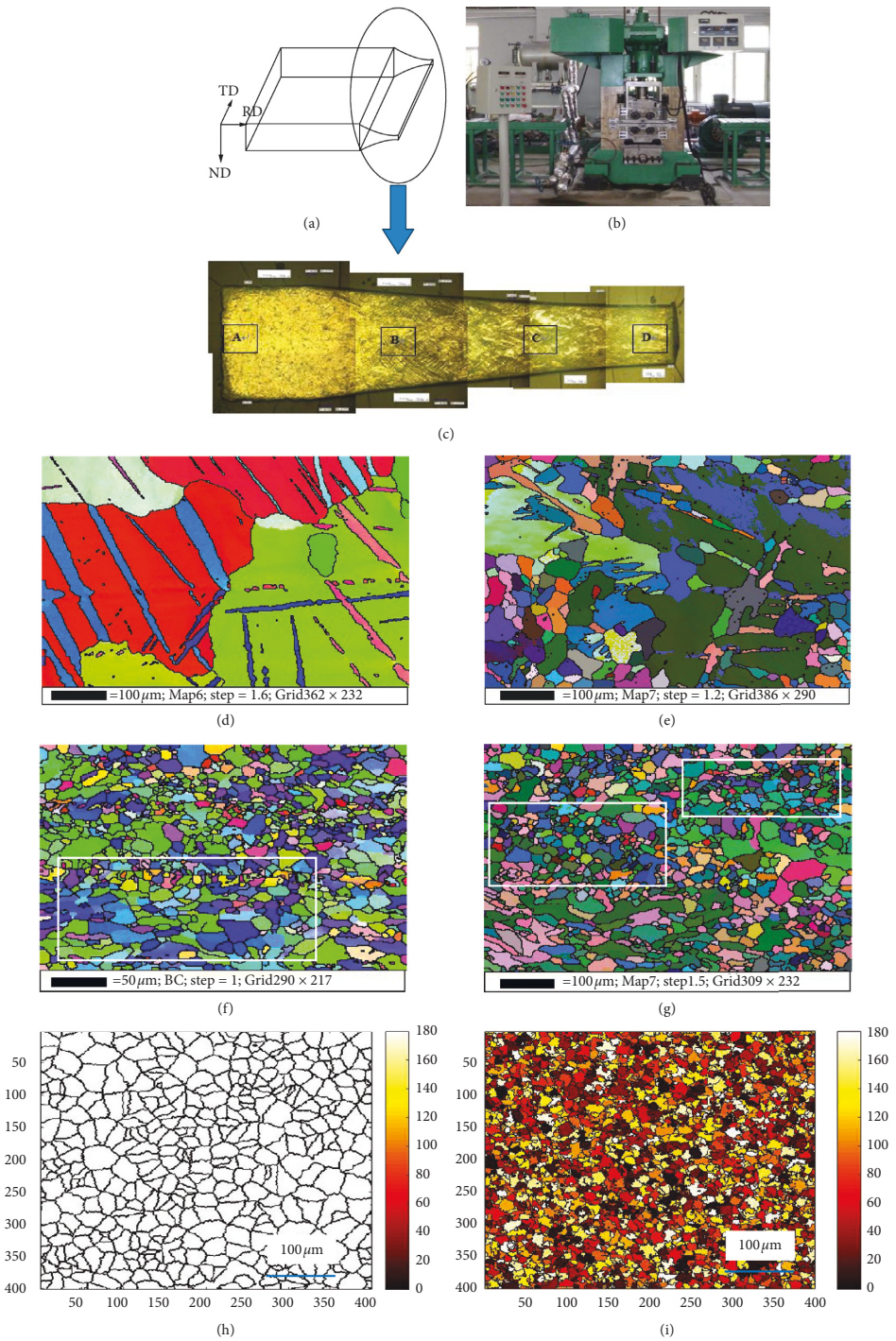

Figure 10: Rolled microstructures in the biting zone of the AZ31 magnesium alloy: (a) rolling sketch image; (b) six roller warm rolling mill; (c) microstructure of the deformation zone; (d) coarse twin grains in the A zone via EBSD experimental observation; (e) coarse grains after extrusion crushing in the B zone via EBSD experimental observation; (f) coarse grains after extrusion crushing in the C zone via EBSD experimental observation; (g) recrystallizedfine grains in the D zone via EBSD experimental observation; (h) simulated initial grains using the CA method; (i) simulated recrystallized fine grains using the CA method.

substantially changed with the strain rate and temperature; however, the strain has little effect on the mean sizes of the *R*-grains, which means that the *R*-grain size depends on the Zener–Hollomon parameter, which is consistent with the DRX research of grain size [31].

The above results show that the percentage of DRX depends on three factors, namely, strain rate, strain, and temperature. The suitable parameters are helpful for enhancing the percentage of DRX in the hot-rolling AZ31 magnesium alloy sheet.

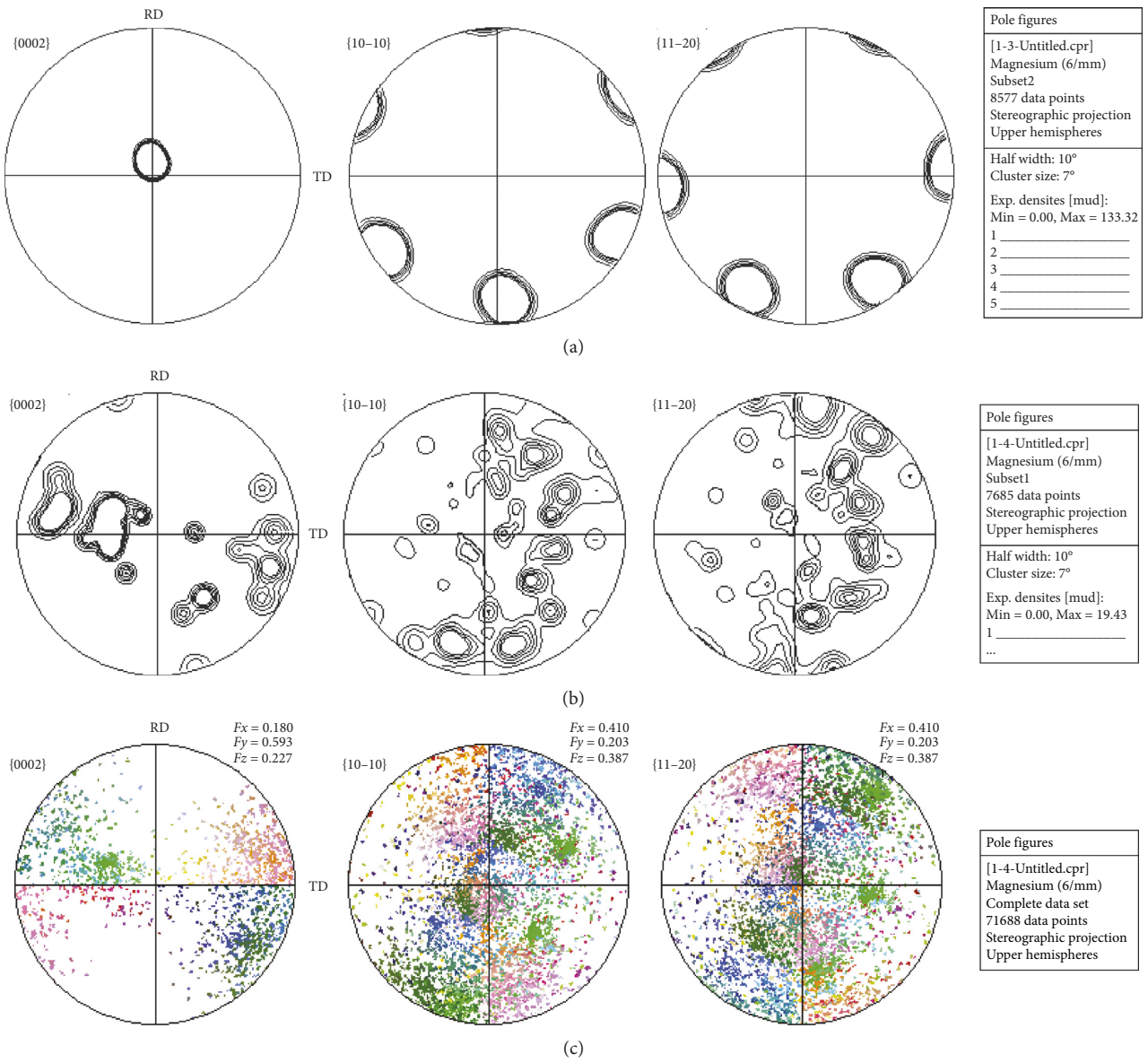

Figure 11: (a) Pole figures of unrolled of A zone; (b) pole figures of the rolled D zone; (c) scatter figures of the rolled D zone.

5. Experiment

The experimental material is made of a unidirectionally solidified AZ31 magnesium alloy composed of 3.0% Al, 1.0% Zn, and 0.2% Mn. The margin composition is Mg, and the rolling experiments were carried out consistent with the simulated data.

Figure 10(a) shows the rolling directions, and Figure 10(b) shows the six roller warm rolling mill. The rolling deformation temperature is 280°C. Comparison of Figures 10(d)–10(g) according to the A–D zones in Figure 10(c) indicates that when the deformation reached the stable rolling deformation, almost all the large twinning grains recrystallized into minute grains. At last, the microstructure of magnesium alloys produced completely recrystallized grains in the large deformation state, and no evident twinning texture was present, which is consistent with the results of the CA method.

It can be seen from Figures 10(d)–10(f) that the grain elongation is the main mechanism during the initial rolling stage due to the influence of rolling force. However, it can be seen from Figure 10(g) that the grain refinement mechanism is obvious at the later stage of rolling because recrystallization plays a major role. As shown in Figure 10(d), the original grain size is more than 100 μm, and there exits coarse twin grains. In order to obtain recrystallized grains, it is necessary to heat up, extrude, and crush them. The crushed initial coarse grain size for recrystallization simulation cannot be obtained directly by experimental method, so the improved CA method was used. Figures 10(h) and 10(i) are the simulation results compared with the experimental results of Figures 10(f) and 10(g).

By comparing and analyzing Figure 10, numerous initial twin structures in the AZ31 unidirectional solidified sheet itself were found. The recrystallized grains nucleate at the twin boundary and the original grain boundary until the twins were completely replaced by the recrystallized grains. No distinction was found between the twin boundary and the original grain boundary in this paper. The recrystallization mechanism is based on the grain boundary bulging. The recrystallized grains nucleated at the grain boundaries with the increase of deformation and developed into the original grain boundaries until the matrix was completely replaced by the fine recrystallized grains. The twin boundaries and primitive boundaries provide the necessary core position and energy for nucleation during deformation, which is due to the accumulation of dislocations at these locations that were hindered by the twin or primitive grain boundaries during deformation. The increasing density of the local dislocations is necessary for the recrystallized grain nucleation. The recrystallized grains, which first formed and grew up, will also deform synchronously with the matrix with the further increase of deformation. Once the dislocation density at the grain boundary reaches the critical value, recrystallization will occur, which will further refine the recrystallized grains.

Figure 11 shows that the anisotropy of grain orientation is strong before rolling; however, the grain orientation was dispersed after rolling. Also, the anisotropy was weakened. Based on the above results, it can be concluded that the small amount of deformation leads to the twinning microstructure with large grains. The magnesium alloy can obtain complete recrystallized grains when the rolling deformation increases, and the complete DRXed microstructure will decrease the flow stress to soften the magnesium sheet, thus achieving a weakening texture of the magnesium alloy sheet.

6. Conclusions

(1) A constitutive model coupled stress variable was established for the unidirectional solidification sheet of AZ31 magnesium alloys and to predict the DRX microstructural evolution of AZ31 magnesium alloys. The approach provides a multiscale modeling to bridge the macroscopic rolling process analysis with the microscopic DRX activities and achieve a weakening texture of the magnesium alloy sheet.

(2) By the bulging nucleation mechanism of DRX and coupling the CA method and the metallurgical principles, the grain refinement of DRXed grains was successfully acquired. The appropriate parameters during the rolling process, which were discussed in detail in this paper, are helpful for enhancing the percentage of DRX. The recrystallized microstructure obtained via the CA method is in good agreement with the EBSD experiment.

Data Availability

The data used to support the findings of this study are available from the corresponding author upon request.

Conflicts of Interest

The authors declare that they have no conflicts of interest.

Acknowledgments

This research was financially supported by the Project of Education Department of Liaoning Province (2016HZPY04) and Science and Technology Department of Liaoning Province (20170520313). The authors wish to thank Casting and Rolling Research Center of Magnesium Alloy at the University of Science and Technology Liaoning.

References

[1] K. Huang and R. E. Logé, "A review of dynamic recrystallization phenomena in metallic materials," *Materials & Design*, vol. 111, pp. 548–574, 2016.

[2] M. G. Jiang, C. Xu, H. Yan et al., "Unveiling the formation of basal texture variations based on twinning and dynamic recrystallization in AZ31 magnesium alloy during extrusion," *Acta Materialia*, vol. 157, pp. 53–71, 2018.

[3] K. D. Molodov, T. Al-Samman, D. A. Molodov, and G. Gottstein, "Mechanisms of exceptional ductility of magnesium single crystal during deformation at room temperature: multiple twinning and dynamic recrystallization," *Acta Materialia*, vol. 76, pp. 314–330, 2014.

[4] A. Galiyev, R. Kaibyshev, and G. Gottstein, "Correlation of plastic deformation and dynamic recrystallization in magnesium alloy Zk60," *Acta Materialia*, vol. 49, no. 7, pp. 1199–1207, 2001.

[5] R. Ding and Z. X. Guo, "Coupled quantitative simulation of microstructural evolution and plastic flow during dynamic recrystallization," *Acta Materialia*, vol. 49, no. 16, pp. 3163–3175, 2001.

[6] R. Ding and Z. X. Guo, "Microstructural evolution of a Ti-6Al-4V alloy during β-phase processing: experimental and simulative investigations," *Materials Science and Engineering: A*, vol. 365, no. 1-2, pp. 172–179, 2004.

[7] L. Guo and F. Fujita, "Modeling the microstructure evolution in AZ31 magnesium alloys during hot rolling," *Journal of Materials Processing Technology*, vol. 255, pp. 716–723, 2018.

[8] J. Hou, M. Zhang, H. Yang, and J. Qiao, "Deformation behavior of $Al_{0.25}CoCrFeNi$ high-entropy alloy after recrystallization," *Metals*, vol. 7, no. 4, p. 111, 2017.

[9] Y. Huang, S. Wang, Z. Xiao, and H. Liu, "Critical condition of dynamic recrystallization in 35CrMo steel," *Metals*, vol. 7, no. 5, p. 161, 2017.

[10] A. Manonukul and F. P. E. Dunne, "Initiation of dynamic recrystallization under inhomogeneous stress states in pure copper," *Acta Materialia*, vol. 47, no. 17, pp. 4339–4354, 1999.

[11] R. L. Goetz and V. Seetharaman, "Modeling dynamic recrystallization using cellular automata," *Scripta Materialia*, vol. 38, no. 3, pp. 405–413, 1998.

[12] F. Chen, Z. S. Cui, J. Liu, X. X. Zhang, and W. Chen, "Modeling and simulation on dynamic recrystallization of 30Cr2Ni4MoV rotor steel using the cellular automaton method," *Modelling and Simulation in Materials Science and Engineering*, vol. 17, article 075015, 2009.

[13] X. H. Deng, L. W. Zhang, and C. X. Yue, "Influence of hot working parameters on dynamic recrystallisation of GCr15 bearing steel," *Materials Research Innovations*, vol. 13, no. 4, pp. 436–440, 2009.

[14] S.-q. Huang, Y.-p. Yi, and C. Liu, "Simulation of dynamic recrystallization for aluminium alloy 7050 using cellular automaton," *Journal of Central South University of Technology*, vol. 16, no. 1, pp. 18–24, 2009.

[15] X. Li, X. Li, H. Zhou, X. Zhou, F. Li, and Q. Liu, "Simulation of dynamic recrystallization in AZ80 magnesium alloy using cellular automaton," *Computational Materials Science*, vol. 140, pp. 95–104, 2017.

[16] G. Kugler and R. Turk, "Modeling the dynamic recrystallization under multi-stage hot deformation," *Acta Materialia*, vol. 52, no. 15, pp. 4659–4668, 2004.

[17] A. Yanagida and J. Yanagimoto, "A novel approach to determine the kinetics for dynamic recrystallization by using the flow curve," *Journal of Materials Processing Technology*, vol. 151, no. 1-3, pp. 33–38, 2004.

[18] C. M. Sellars and W. J. Tegart, "La relation entre la résistance et la structure dans la deformation à chaud," *Mémoires Scientifiques de la Revue de Metallurgie*, vol. 63, pp. 731–746, 1966.

[19] H. J. McQueen and N. D. Ryan, "Constitutive analysis in hot working," *Materials Science and Engineering: A*, vol. 322, no. 1-2, pp. 43–63, 2002.

[20] R. Bhattacharya, Y. J. Lan, B. P. Wynne, B. Davis, and W. M. Rainforth, "Constitutive equations of flow stress of magnesium AZ31 under dynamically recrystallizing conditions," *Journal of Materials Processing Technology*, vol. 214, no. 7, pp. 1408–1417, 2014.

[21] H. J. McQueen, S. Yue, N. D. Ryan, and E. Fry, "Hot working characteristics of steels in austenitic state," *Journal of Materials Processing Technology*, vol. 53, no. 1-2, pp. 293–310, 1995.

[22] H. Mirzadeh, "Constitutive analysis of Mg-Al-Zn magnesium alloys during hot deformation," *Mechanics of Materials*, vol. 77, pp. 80–85, 2014.

[23] H. Mirzadeh, "Constitutive behaviors of magnesium and Mg-Zn-Zr alloy during hot deformation," *Materials Chemistry and Physics*, vol. 152, pp. 123–126, 2015.

[24] H. Mirzadeh, M. Roostaei, M. H. Parsa, and R. Mahmudi, "Rate controlling mechanisms during hot deformation of Mg-3Gd-1Zn magnesium alloy: dislocation glide and climb, dynamic recrystallization, and mechanical twinning," *Materials & Design*, vol. 68, pp. 228–231, 2015.

[25] H. N. Lee, S. T. Chang, H. S. Ryoo, and S. K. Hwang, "Topology and grain size distribution of a two dimensional microstructure produced by a computer tessellation method," *Metals and Materials*, vol. 4, no. 1, pp. 67–73, 1998.

[26] F. J. Humphreys, "A unified theory of recovery, recrystallization and grain growth, based on the stability and growth of cellular microstructures-II. The effect of second-phase particles," *Acta Materialia*, vol. 45, no. 12, pp. 5031–5039, 1997.

[27] W. T. Read and W. Shockley, "Dislocation models of crystal grain boundaries," *Physical Review*, vol. 78, no. 3, pp. 275–289, 1950.

[28] Y. J. Kim, S. K. Hwang, M. H. Kim, S. I. Kwun, and S. W. Chae, "Three-dimensional Monte-Carlo simulation of grain growth using triangular lattice," *Materials Science and Engineering: A*, vol. 408, no. 1-2, pp. 110–120, 2005.

[29] H. Mecking and U. F. Kocks, "Kinetics of flow and strain-hardening," *Acta Metallurgica*, vol. 29, no. 11, pp. 1865–1875, 1981.

[30] W. Roberts and B. Ahlblom, "A nucleation criterion for dynamic recrystallization during hot working," *Acta Metallurgica*, vol. 26, no. 5, pp. 801–813, 1978.

[31] B. Derby, "The dependence of grain size on stress during dynamic recrystallisation," *Acta Metallurgica et Materialia*, vol. 39, no. 5, pp. 955–962, 1991.

[32] N. Xiao, C. Zheng, D. Li, and Y. Li, "A simulation of dynamic recrystallization by coupling a cellular automaton method with a topology deformation technique," *Computational Materials Science*, vol. 41, no. 3, pp. 366–374, 2008.